ELSEVIER

Contents lists available at ScienceDirect

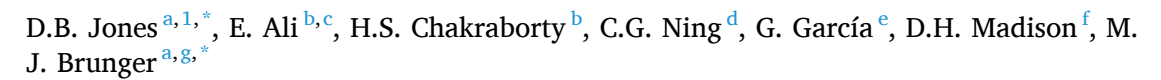
# **Chemical Physics Letters**

journal homepage: www.elsevier.com/locate/cplett



# Research paper

# A dynamical (e,2e) investigation into the ionization of pyrazine



- <sup>a</sup> College of Science and Engineering, Flinders University, GPO Box 2100, Adelaide, SA 5001, Australia
- b Department of Natural Sciences, D. L. Hubbard Center for Innovation, Northwest Missouri State University, Maryville, MO 64468, USA
- <sup>c</sup> Department of Physics, Faculty of Arts & Sciences-El Marj, University of Benghazi, El Marj, Libya
- d Department of Physics, State Key Laboratory of Low-Dimensional Quantum Physics, Tsinghua University, Beijing 100084, China
- <sup>e</sup> Instituto de Física Fundamental, Consejo Superior de Investigaciones Científicas (CSIC), Serrano 113-bis, 28006 Madrid, Spain
- f Department of Physics, Missouri University of Science and Technology, Rolla, MO 65409, USA
- g Department of Actuarial Science and Applied Statistics, Faculty of Business and Management, UCSI University, Kuala Lumpur 56000, Malaysia

#### ARTICLE INFO

### Keywords: Electron ionization Pyrazine Scattering dynamics

#### ABSTRACT

We report an experimental and theoretical investigation into the dynamics of electron-impact ionization of the unresolved outermost molecular orbitals  $(6a_g+1b_{1g})$  of pyrazine  $(C_4N_2H_4)$ . Experimental triple differential cross sections (TDCS) are compared with cross sections calculated within a molecular 3-body distorted wave (M3DW) framework. The M3DW theory was able to reproduce the qualitative scattering behaviour in the binary region, but failed to describe the absolute intensity of the TDCS and the recoil scattering behaviour. Momentum profiles were used to identify possible sources where the M3DW may mask the quantum character of the ionized orbitals in describing the ionization dynamics.

# 1. Introduction

Radiation-based therapies involve exposing biological systems to primary ionizing particles that deposit their energy through successive collisional interactions with the molecular constituents. Simulations of charged-particle tracks through liquid water, a surrogate for soft biomaterials, provide insights into the early physical and chemical radiation actions on matter [1]. It has been demonstrated that the secondary electrons produced in the primary ionization events can potentially damage DNA, even at low impact energies [2]. Thus, in order to characterise all DNA-damaging events, it is essential to understand how all primary and secondary particles are transported and deposit energy in media other than pure liquid water, to more appropriately represent real biological systems.

For charged-particle transport [3,4], plasma [5] or radiative modelling [6] it is necessary to have complete cross section libraries that describe the likelihood of each scattering process [7–9], and that cover the full range of accessible energies found within the environment to be simulated. To meet these demands, it is essential that developed theoretical models are predictive and applicable to a broad range of

biomolecules over a large range of collisional regimes. We have therefore focused on trying to understand the role of molecular structure in the dynamics of electron scattering [7]. As a part of this work, we have performed systematic experimental and theoretical investigations into the electron impact ionization of biomolecules, with different functional groups, under coplanar asymmetric scattering conditions at intermediate impact energies in order to investigate the role that structure plays in the collision dynamics [10-13]. This experimental work has been essential in developing and refining theoretical models and approximations that enable the calculation of ionization cross sections of complex molecular species. A number of different theoretical models have now emerged that are applicable within this regime, which includes the molecular 3-body distorted wave (M3DW) calculations, distorted-wave first Born approximation calculations [14-17] and multicentre distorted wave calculations [18-20]. These methods have all revealed the importance in performing a proper average over the molecular orientation, in the calculated triply differential cross sections, when comparing to experimental data where the molecular orientation is undefined. While these theoretical methods have largely addressed the characteristic shapes of observed triple differential cross sections

<sup>\*</sup> Corresponding authors.

 $<sup>\</sup>textit{E-mail addresses: } darryl.jones@flinders.edu.au (D.B. Jones), \\ michael.brunger@flinders.edu.au (M.J. Brunger).$ 

<sup>1</sup> Present address: Flinders Microscopy and Microanalysis, College of Science and Engineering, Flinders University, GPO Box 2100, Adelaide, SA 5001, Australia.

(TDCS), questions still remain about their intensity for the calculated TDCS, with experimental TDCS angular distributions typically being obtained on a relative scale. Recently, experimental TDCS for complex molecules have been inter-normalised [21,22] or fully captured in reaction microscopes [23], so that we can now begin to assess the intensity scales of theoretical TDCS for complex molecular systems.

To further contribute to this work, we now present results from an investigation into pyrazine ( $C_4N_2H_4$ ). Pyrazine is an azabenzene, having strong similarities to the DNA base analogue pyrimidine, with the ionization of pyrimidine having been the subject of numerous experimental and theoretical investigations [16,24,25]. The present investigation therefore enables an evaluation of how the location of the nitrogen atoms, within the 6-membered ring, influences the scattering process, thereby continuing our efforts to understand the role of structure in electron scattering reactions.

As a prototypical biomolecule, pyrazine has been the subject of numerous electron scattering studies. Elastic scattering data has been measured by Palihawadana et al. over the 3-50 eV range [26], while theoretical calculations have been performed using the R-matrix [27] and Schwinger Multichannel methods [28]. Those studies have been more recently supplemented by total cross section measurements over the 10-500 eV range [29]. Theoretical calculations have also investigated the nature of resonance structures in the diazines [30]. There have also been recent theoretical investigations of positron collisions with pyrazine [31]. The structural similarity of pyrazine to benzene, and the other azabenzenes, has made its electronic structure the subject of VUV photo absorption [32] and electron impact excitation [32,33] investigations. These works have also been supplemented by theoretical quantum chemical calculations of the excited electronic structure of pyrazine [32,34]. Ionization studies of pyrazine include He (I) UPS in the gas-phase [35,36] and in supersonic jets [37], and synchrotron photoelectron spectroscopic investigations [38]. Non-adiabatic processes in pyrazine have also been investigated using time-resolved photoelectron spectroscopy, with this reviewed by Suzuki [39].

In the present manuscript we present our results from an investigation into ionization dynamics from pyrazine. In Section II, we provide details of our experimental and theoretical methodologies. This is followed, in Section III, by a presentation and discussion of our results. Lastly, a summary of our findings is presented in Section IV.

# 2. Experimental and theoretical details.

An (e,2e) coincidence technique was employed to obtain triple differential cross sections for the electron impact ionization of pyrazine. This kinematically complete ionization reaction can be described through:

$$e_0^-(E_0, \mathbf{k}_0) + T_{Pyrz} \rightarrow T_{Pyrz}^+(\mathbf{\epsilon}_i, \mathbf{q}) + e_1^-(E_1, \mathbf{k}_1) + e_2^-(E_2, \mathbf{k}_2)$$
 (1)

Here an electron with well-defined energy  $(E_0)$  and momentum  $(k_0)$  is incident on and collides with a pyrazine target molecule  $(T_{Pyrz})$  at rest. The ionizing collision produces a fast scattered  $(e_1^-)$  and slow ejected  $(e_2^-)$  electron with well-defined energies  $(E_1,E_2)$  and momenta  $(k_1,k_2)$ , respectively. Conservation of energy in the collision requires,

$$\epsilon_i = E_0 - (E_1 + E_2) \tag{2}$$

where  $\epsilon_i$  is the energy needed to remove the bound electron from the pyrazine molecule to produce a residual pyrazine ion,  $T^+_{Pyrz}(\epsilon_i, q)$ . To conserve momentum in this collision, this ion recoils with momentum q.

The TDCS is observed under asymmetric energy sharing coplanar kinematics, where the energies of the incident ( $E_0=250~\rm eV$ ) and ejected ( $E_2=20~\rm eV$ ) electrons are fixed, and the angles of the electrons, made with reference to the incident electron direction, varies. Here the energy of the scattered electron is selected to conserve energy in the ionization of the unresolved highest occupied molecular orbital and next highest

occupied molecular orbital (HOMO + NHOMO) of pyrazine. In the collision, we define the momentum transferred to the target by:

$$K = k_0 - k_1. \tag{3}$$

Under these kinematics, the momentum transfer magnitude increases with the changing scattered electron angle from  $\theta_1=-5$  to  $-15^\circ$ . Here the momentum transfer magnitude is typically less than or close to that of the slow outgoing electron  $|\mathbf{K}| \leq |k_2|$ , so that the TDCS angular distribution is particularly sensitive to the collisional scattering dynamics. In discussing TDCS angular distributions, we refer to binary collisions and regions, where the momentum vector of the ejected electron is close to being parallel to the momentum transfer direction (+K). We also refer to recoil scattering, where the ejected electron leaves the collision at angles close to being antiparallel to the momentum transfer direction (-K).

Our experiments are performed in an experimental apparatus that has been described by Cavanagh and Lohmann [40]. Briefly, a fixed energy electron beam is formed by the collimation of thermionic electrons emitted from a tungsten filament in an electron gun. The electron beam intersects an effusive beam of pyrazine, flowing into the collision region through a beam forming needle. Here the pyrazine vapour is obtained from a solid pyrazine sample (Sigma-Aldrich, purity > 99%) at room temperature. Note that this solid pyrazine sample had been degassed using repeated freeze-pump cycles, and that the vapour flowing into the chamber through the needle is controlled using a variable leak valve. Here the vacuum chamber pressure used for the experiments was typically less than  $5 \times 10^{-6}$  torr. The vacuum chamber itself was heated to  $\sim 30$  °C to prevent deposition of the pyrazine vapour on the walls of the chamber. Electrons scattering from the pyrazine target were detected using two electron analysers that are mounted on independently rotatable turntables. Each analyser is comprised of a set of electrostatic lenses, electron energy selecting hemispheres, and a channel electron multiplier [40].

Binding energy spectra (BES) for pyrazine were obtained by observing the coincident count rate, while scanning over a range of scattered electron energies and keeping the incident ( $E_0=250~{\rm eV}$ ) and slow scattered electron ( $E_2=20~{\rm eV}$ ) energies fixed. Here the scattered and ejected electron detection angles (made with respect to the incident electron direction) were also fixed at  $-10^\circ$  and  $75^\circ$ , respectively. The binding energy spectrum was used to identify the scattered electron energy (and thus binding energy) corresponding to the ionization of the unresolved HOMO + NHOMO ( $6a_g+1b_{1g}$ ) of pyrazine, with an example of a present BES being given in Fig. 1.

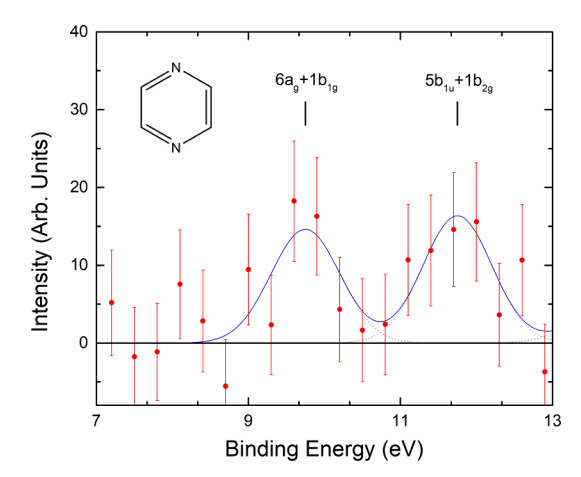


Fig. 1. Experimental binding energy spectra for pyrazine. Here the incident and slow ejected electron energies were fixed at 250 and 20 eV, respectively. The fast scattered and slow ejected electrons were detected at  $\theta_1=$  -10° and  $\theta_2=75^\circ$ , respectively. The grey dotted curves are Gaussian functions used to fit the resolvable experimental features, and the blue curve is their sum.

Triple differential cross sections (TDCS) were subsequently recorded by fixing the detection energy of the scattered electron analyser, so that it matched the ionization of the unresolved HOMO + NHOMO, noting that our coincidence energy resolution of  $\sim 1.1\,$  eV is insufficient to uniquely resolve the HOMO and NHOMO. Angular distributions of the TDCS were finally obtained by recording the coincidence count rate for a fixed detection angle of the fast-scattered electrons, and then scanning over relevant angular ranges of the ejected electrons. TDCS for different scattered electron angles were then inter-normalized by fixing the ejected electron angle and scanning the TDCS over the scattered electron angles. Under these experimental conditions, the TDCS was recorded in a binning mode [41] to account for any variations in electron beam current and the target density in the interaction region during the measurements.

Theoretical cross sections for the pyrazine HOMO and NHOMO were calculated using the M3DW method, that has been described previously [25,42–44]. Within this framework, the transition matrix is evaluated for a molecular orientation of the pyrazine target (*R*),

$$T_{dir}(\mathbf{R}) = \langle \chi_1^-(\mathbf{k}_1, \mathbf{r}_1) \chi_2^-(\mathbf{k}_2, \mathbf{r}_2) C_{12}(\mathbf{r}_{12}) | V_0 - U_0 | \phi_{Dv}(\mathbf{r}_2, \mathbf{R}) \chi_0^+(\mathbf{k}_0, \mathbf{r}_1) \rangle. \tag{4}$$

Here  $\chi_0^+(k_0,r_1)$ ,  $\chi_1^-(k_1,r_1)$  and  $\chi_2^-(k_2,r_2)$  are distorted waves for the incident, scattered and ejected electrons, respectively.  $C_{12}(r_{12})$  is the Coulomb post-collision interaction factor between the two outgoing electrons. In the above expression,  $r_1$  and  $r_2$  correspond to the positions of the initially incident and bound electrons, respectively, while  $r_{12}$  is the distance between the two electrons. Here,  $V_0$  and  $U_0$  describe the electron-target interaction and distorting potentials, respectively. Lastly,  $\phi_{Dy}(r_2,R)$  is the one electron Dyson orbital [43]. The TDCS for an oriented molecule is then obtained through,

$$\frac{d^{5}\sigma}{d\Omega_{1}d\Omega_{2}dE}(\mathbf{R}) = \frac{1}{\left(2\pi\right)^{5}} \frac{k_{1}k_{2}}{k_{0}} \left(\left|T_{dir}(\mathbf{R})\right|^{2} + \left|T_{exc}(\mathbf{R})\right|^{2} + \left|T_{dir}(\mathbf{R}) - T_{exc}(\mathbf{R})\right|^{2}\right)$$
(5)

Here  $T_{exc}(R)$  is the exchange amplitude, which is calculated in the same way as the direct scattering amplitude (eq. (4)) but with an interchange of the scattered and ejected electron coordinates in the final state. In the present experimental work, the orientation of the molecules during the collision is unknown. Therefore, to directly compare the theoretical and experimental TDCS, the theoretical cross sections are averaged over all possible molecular orientations in order to account for the unknown orientation of the molecule during the collision. In this work, the proper averaged TDCS,

$$\frac{d^{5}\sigma^{PA}}{d\Omega_{1}d\Omega_{2}dE} = \frac{\int \frac{d^{5}\sigma}{d\Omega_{1}d\Omega_{2}dE}(\boldsymbol{R})d\Omega_{R}}{\int d\Omega_{R}},\tag{6}$$

is obtained by evaluating the M3DW TDCS at specific molecular orientations and performing a numerical integration. Theoretical cross sections reported in the present work are in atomic units (a.u.) and are differential with respect to the solid angles of the scattered and ejected electrons and their energy sharing in the ionization process.

To assist in the interpretation of the experimental data, we have additionally performed quantum chemical calculations to derive spectroscopic details about pyrazine, and the related azabenzene pyrimidine. These calculations included optimizing the molecular geometries at the B3LYP/aug-cc-pVDZ level and performing single point energy calculations using that same Density Functional Theory (DFT) level. All of these calculations were performed in Gaussian 09 [45], and they allowed us to calculate momentum profiles [41] for the orbitals that were ionized [46].

### 3. Results and discussion

A typical binding energy spectrum for pyrazine is presented in Fig. 1, with the present ionization energies of pyrazine being presented in

**Table 1** Experimental and theoretical binding energies  $(\epsilon)$  of pyrazine, and their spectroscopic assignments. <sup>(a)</sup> The ordering of the symmetry axes has been changed for consistency in the orbital assignments.

Present Expt.			PES	PES	OVGF/ cc-	P3/ cc-
∈(eV)	Assign.	Assign.	[37]	[38]	pVDZ [47] <sup>(a)</sup>	pVTZ [47] <sup>(a)</sup>
9.75	6a <sub>g</sub> + 1b <sub>1g</sub>	6a <sub>g</sub> (n)	9.288	8.70-9.95	9.234	9.788
	_	$1b_{1g}(\pi)$	10.169	9.95-10.80	9.763	10.290
11.75	$5b_{1u} + 1b_{2g}$	5b <sub>1u</sub> (n)		10.80–11.35	11.164	11.573
	<u> </u>	$1b_{2g}(\pi)$		11.35–12.75	11.497	12.013

Table 1 where they are compared with previously reported theoretical and experimental values. In our BES, we observe a band for the unresolved HOMO and NHOMO ( $6a_g+1b_{1g}$ ), which is well separated from the next feature, assigned to the unresolved ( $5b_{1u}+1b_{2g}$ ) orbitals. Our results are consistent with the interpretation of the photoemission electron spectra (PES), which with its higher resolution are also able to resolve the HOMO ( $6a_g$ ) and NHOMO ( $1b_{1g}$ ). Ortiz and Zakrzewski [47] carried out calculations for the ionization energies, using outer valance Green's function (OVGF) and Partial 3rd order (P3) methods, with the assignments and position of the spectral features being in good accord with the experimental data. The central position of the unresolved ( $6a_g+1b_{1g}$ ) orbitals, through the conservation of energy, sets the scattered electron energy we employed for undertaking the TDCS angular distribution measurements.

The TDCS angular distributions for the ionization of the unresolved  $(6a_g+1b_{1g})$  orbitals are presented in Fig. 2. Here we experimentally observed, in the  $\theta_1=-10^\circ$  and  $-15^\circ$  angular distributions, that the TDCS in the binary region suggests a weak minimum at or near the momentum

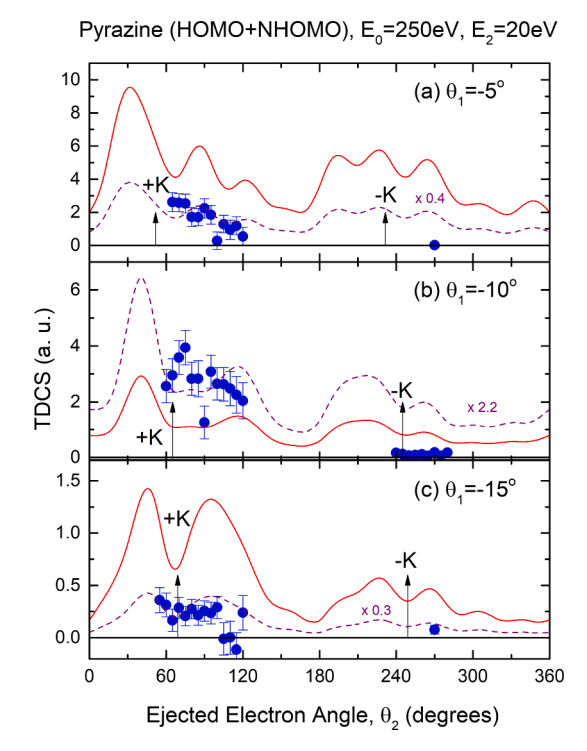


**Fig. 2.** Experimental and theoretical TDCS for ionization of the unresolved HOMO + NHOMO  $(6a_g+1b_{1g})$  of pyrazine, obtained for incident and ejected electron energies of 250 eV and 20 eV, respectively. Here the fast-scattered electron was detected at (a)  $-5^{\circ}$ , (b)  $-10^{\circ}$ , and (c)  $-15^{\circ}$ . Solid curves indicate theoretical data while dashed curves indicate data that has been rescaled. See text for further details.

transfer direction in the angular distributions, with the TDCS intensity subsequently reaching a plateau or increasing for the larger ejected electron angles. The intensity of this broad binary lobe, in all the observed TDCS angular distributions, does drop off at the angles far  $(\sim\!60^\circ)$  from the momentum transfer direction. Finally, we note that the experimental distributions do not show any evidence for any significant recoil peak structure.

We now compare the M3DW theory to the experimental data (again see Fig. 2). Here the experimental TDCS angular distributions have been internormalised, so that the TDCS have been placed onto the absolute scale, using a single point normalisation to the theoretical M3DW calculations. From this, we can observe that the relative intensity of the calculations does not match that which we observe experimentally. Theoretically, the M3DW predicts a binary region intensity that decreases as the scattered electron angle changes from,  $\theta_1=$ -5° to  $-15^\circ$ . Experimentally, we see that the intensity is comparable for the  $\theta_1=$ -5° and  $-10^\circ$  binary-region angular distributions, before dropping when the scattered electron detector moves to  $\theta_1=$ -15°. The experimental distribution therefore doesn't display the same intensity decrease in the binary region seen in the theoretical calculations, as the momentum transfer to the target increases.

To assess the shape of the theoretical TDCS, each angular distribution has been independently renormalised to the experimental data (with the relevant scaling factors also shown in Fig. 2). Here the theoretical distributions do a reasonable job at reproducing the gross scattering behaviour observed in the binary region, but the theory does suggest some smaller structures in the TDCS that are not consistent with the experimental observations. In particular, we see a local maximum in the measured TDCS, where the ejected electrons are emitted at angles slightly larger than the momentum transfer direction in the  $\theta_1=$ -5° and  $-10^\circ$  angular distributions, while the theory suggests a local lower intensity region.

Recently, there has been interest in understanding the role of molecular structure in the ionization dynamics, with investigations indicating the important role played by the orbital that is ionized [48,49]. Builth-Williams et al previously reported a TDCS angular distribution for the ionization of the HOMO (7b<sub>2</sub>) orbital of pyrimidine, under the same asymmetric coplanar kinematics and with a 250 eV impact energy, for a scattered electron angle of  $\theta_1 = -15^\circ$  and a 20 eV ejected electron energy [24]. This work was recently revisited, with new theoretical calculations employing the proper averaged M3DW theory [25]. In order to discuss the role of structure in the TDCS, M3DW calculations for the  $6a_g$  and  $1b_{1g}$  orbitals of pyrazine and the  $7b_2$  orbital of pyrimidine [25] are presented in Fig. 3. To further assist in understanding the role of structure in the calculations, we also present the orbital momentum profiles for all the relevant orbitals in Fig. 4.

In the theoretical TDCSs, we observe in Fig. 3 significant variations in the intensity scales for each orbital considered. Here the pyrazine  $6a_g$ orbital gives the biggest intensity, followed by the 7b2 orbital of pyrimidine, and lastly the 1b<sub>1g</sub> orbital of pyrazine. When considering the orbital characters and momentum profiles (see Fig. 4), the 7b2 pyrimidine orbital has strong similarities to the pyrazine  $6a_g$  orbital, with both orbitals exhibiting a nitrogen p-character that couples to the  $\sigma$  carbon frame. In pyrimidine the location of the nitrogen atoms in the 1,3 positions leads to a parity inversion between the nitrogen p-characters and the  $\sigma$  carbon frame contributions, compared to that for pyrazine where the parity of the nitrogen (1,4 positions) p-like character is matched. In pyrazine, this orbital parity gives rise to a small 's-character' (i.e. a finite intensity at zero momentum) in the momentum profile. The theoretically weakest TDCS of the pyrazine  $1b_{1g}$  orbital originates from the highly delocalised  $\pi$ -bonding orbital. This delocalisation reduces the cross section intensity in the binary region, and also prevents any substantial recoil scattering. That latter observation is entirely consistent with previous results from other orbitals with a delocalised  $\pi$ -bonding character, such as those in phenol [50].

The momentum profiles [41] for all the orbitals investigated in

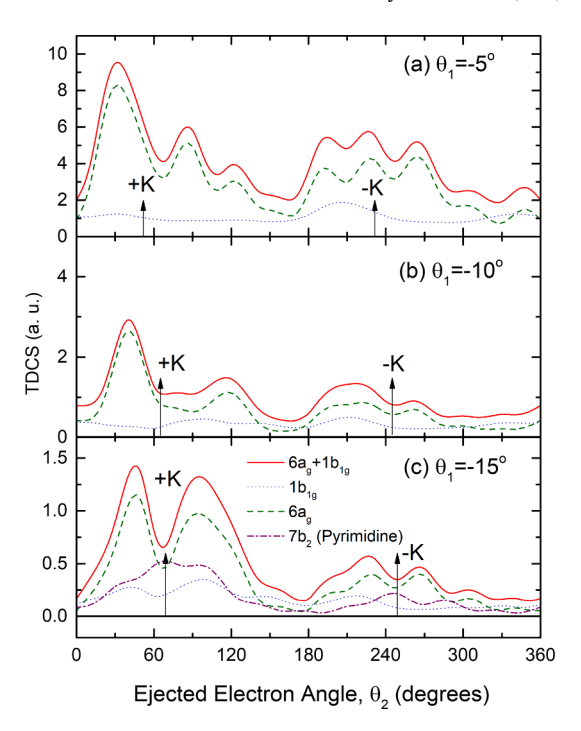


**Fig. 3.** Theoretical TDCS for ionization of the HOMO  $(6a_g)$ , NHOMO  $(1b_{1g})$ , and HOMO + NHOMO  $(6a_g+1b_{1g})$  of pyrazine, obtained for incident and ejected electron energies of 250 eV and 20 eV, respectively. Here the fast-scattered electron was detected at (a)  $-5^\circ$ , (b)  $-10^\circ$ , and (c)  $-15^\circ$ . Also shown is the TDCS for the HOMO  $(7b_2)$  of the structurally similar molecule pyrimidine. See text for further details.

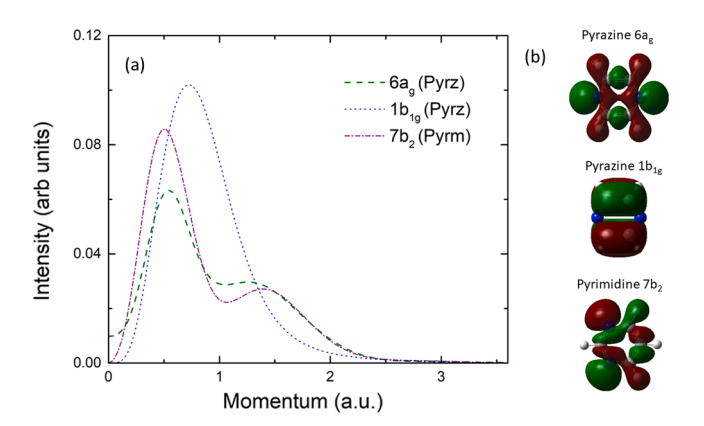


**Fig. 4.** (a) Theoretical momentum profiles and (b) diagrammatic representations of the HOMO ( $6a_g$ ), and NHOMO ( $1b_{1g}$ ) of pyrazine and the HOMO ( $7b_2$ ) of pyrimidine. See text for further details.

pyrazine and pyrimidine display strong p-characters, with the maximum intensity being found away from zero momentum (see Fig. 4). The behaviour of the momentum profile is often reflected in the binary region of the experimental TDCSs, under kinematics approaching the Bethe ridge, where the momentum transfer magnitude is comparable to that for the ejected electron ( $\theta_1 = -15^{\circ}$  in our kinematics). Under these conditions, the behaviour of the TDCS at the momentum transfer direction corresponds to the near zero component of the momentum profile. As the ejected electron angle moves away from the +K direction, the momentum that the bound electron had when it was ionized should increase so that the TDCS should mimic the behaviour of the momentum profile. Indeed, the experimental TDCS for the unresolved  $(6a_g + 1b_{1g})$  orbitals of pyrazine and the  $7b_2$  orbital of pyrimidine exhibit this behaviour. While the orbital character is indeed reflected in the pyrazine M3DW TDCS, it is not observed in the M3DW TDCS of pyrimidine (see

Fig. 3) as it has maximum intensity on the momentum transfer direction. This observation suggests that the scattering dynamics in the M3DW theory may be masking or losing important aspects of an orbital's character, that will be essential in reproducing the measured ionization behaviour. An inadequate description of such key orbital features may, in part, explain why minor structures in the experimental pyrazine TDCS intensity are not so well reproduced in the theoretical TDCS. It may also contribute to the variations in absolute cross section intensity observed when the scatted electron angle changes. The M3DW calculation, employing the proper average, has made significant progress in describing the complex ionization dynamics, however, there are clearly still aspects of the theoretical description that limits its ability to fully reproduce the experimentally observed TDCS in pyrazine.

### 4. Conclusions

A joint experimental and theoretical investigation into the ionization dynamics of pyrazine has been reported. The theoretical M3DW model was able to provide a reasonable description of the shape of the TDCS in the binary scattering region but failed to reproduce the relative intensity of the experimental TDCS with changing scattered electron angle. As a result, it appears that the physics contained in the M3DW predicts that shape of the cross section much better than the absolute value for this case. Where a comparison could be made in the recoil region, the level of accord between our measured and calculated TDCSs was marginal. Momentum profiles for the ionized orbitals were used to qualitatively explain the characteristic features of the experimentally observed TDCS. We found that their behaviour was not consistently reproduced through the M3DW calculations, which may indicate that aspects of the molecular structure are currently getting suppressed through the theoretical calculations. The testing of the M3DW theory with proper averaging over molecular orientations against experimental data have revealed the improvements over earlier models, but still shows that the model must be further refined to enable a complete description of the ionization process.

## 5. Data availability statement

The data that supports the findings of this study are available within the article.

# **Declaration of Competing Interest**

The authors declare that they have no known competing financial interests or personal relationships that could have appeared to influence the work reported in this paper.

## Acknowledgements

This work has been partially supported by the Australian Research Council through the Discovery Project Grant #DP180101655. GG acknowledges partial financial support from the Ministerio de Ciencia e Innovacion (Project PID2019-104727RB-C21) and CSIC (Project LINKA20085). The research was also supported by US National Science Foundation Grant No. PHY-1806206 (EA, HSC), OAC-1919789 (EA, DM).

# References

- [1] M. Dingfelder, Health Phys. 103 (2012) 590.
- [2] B. Boudaiffa, P. Cloutier, D. Hunting, M.A. Huels, L. Sanche, Science 287 (2000) 1658
- [3] A.I. Lozano, J.C. Oller, D.B. Jones, R.F. da Costa, M.T. do, N. Varella, M.H. F. Bettega, F. Ferreira da Silva, P. Limão-Vieira, M.A.P. Lima, R.D. White, M. J. Brunger, F. Blanco, A. Muñoz, G. García, Phys. Chem. Chem. Phys. 20 (2018) 22368, https://doi.org/10.1039/C8CP03297A.
- [4] J. de Urquijo, M.J.E. Casey, L.N. Serkovic-Loli, D.G. Cocks, G.J. Boyle, D.B. Jones, M.J. Brunger, R.D. White, J. Chem. Phys. 151 (2019), 054309.

- [5] M.A. Ridenti, J. Amorim Filho, M.J. Brunger, R.F. da Costa, M.T. do, N. Varella, M. H.F. Bettega, M.A.P. Lima, Eur. Phys. J. D. 70 (2016) 161, https://doi.org/10.1140/epjd/e2016-70272-8.
- [6] F. Blanco, A. Muñoz, D. Almeida, F. Ferreira da Silva, P. Limão-Vieira, M.C. Fuss, A. G. Sanz, G. García, Eur. Phys. J. D 67 (2013) 199.
- [7] M.J. Brunger, Int. Rev. Phys. Chem. 36 (2017) 333.
- [8] M.U. Bug, W. Yong Baek, H. Rabus, C. Villagrasa, S. Meylan, A.B. Rosenfeld, Radiat. Phys. Chem. 130 (2017) 459.
- [9] L.C. Pitchford, L.L. Alves, K. Bartschat, S.F. Biagi, M.-C. Bordage, I. Bray, C. E. Brion, M.J. Brunger, L. Campbell, A. Chachereau, B. Chaudhury, L. G. Christophorou, E. Carbone, N.A. Dyatko, C.M. Franck, D.V. Fursa, R.K. Gangwar, V. Guerra, P. Haefliger, G.J.M. Hagelaar, A. Hoesl, Y. Itikawa, I.V. Kochetov, R. P. McEachran, W.L. Morgan, A.P. Napartovich, V. Puech, M. Rabie, L. Sharma, R. Srivastava, A.D. Stauffer, J. Tennyson, J. de Urquijo, J. van Dijk, L.A. Viehland, M.C. Zammit, O. Zatsarinny, S. Pancheshnyi, Plasma Process. Polym. 14 (2017) 1600098.
- [10] J.D. Builth-Williams, G.B. da Silva, L. Chiari, D.B. Jones, H. Chaluvadi, D. H. Madison, M.J. Brunger, J. Chem. Phys. 140 (2014), 214312.
- [11] J.D. Builth-Williams, S.M. Bellm, L. Chiari, P.A. Thorn, D.B. Jones, H. Chaluvadi, D. H. Madison, C.G. Ning, B. Lohmann, G.B. da Silva, M.J. Brunger, J. Chem. Phys. 139 (2013), 034306.
- [12] D.B. Jones, J.D. Builth-Williams, S.M. Bellm, L. Chiari, H. Chaluvadi, D. H. Madison, C.G. Ning, B. Lohmann, O. Ingólfsson, M.J. Brunger, Chem. Phys. Lett. 572 (2013) 32.
- [13] S.M. Bellm, J.D. Builth-Williams, D.B. Jones, H. Chaluvadi, D.H. Madison, C. G. Ning, F. Wang, X.G. Ma, B. Lohmann, M.J. Brunger, J. Chem. Phys. 136 (2012), 244301.
- [14] S.M. Bellm, C.J. Colyer, B. Lohmann, C. Champion, Phys. Rev. A 85 (2012), 022710
- [15] L. Mouawad, P.-A. Hervieux, C.D. Cappello, Z.E. Bitar, J. Phys. B: At. Mol. Opt. Phys. 53 (2019), 025202.
- [16] L. Mouawad, P.-A. Hervieux, C. Dal Cappello, J. Pansane, V. Robert, Z. El Bitar, Eur. Phys. J. D 73 (2019) 76.
- [17] L. Mouawad, P.A. Hervieux, C.D. Cappello, J. Pansanel, A. Osman, M. Khalil, Z. E. Bitar, J. Phys. B: At. Mol. Opt. Phys. 50 (2017), 215204.
- [18] X. Xu, M. Gong, X. Li, S.B. Zhang, X. Chen, J. Chem. Phys. 148 (2018), 244104.
- [19] Z. Wang, M. Gong, X. Li, S.B. Zhang, X. Chen, J. Electron Spectrosc. Relat. Phenom. 248 (2021), 147059.
- [20] E. Ali, D. Madison, Phys. Rev. A 100 (2019), 012712.
- [21] D.B. Jones, E. Ali, C.G. Ning, F.F.D. Silva, O. Ingólfsson, M.C.A. Lopes, H. S. Chakraborty, D.H. Madison, M.J. Brunger, J. Chem. Phys. 151 (2019), 124306, https://doi.org/10.1063/1.5123526.
- [22] D.B. Jones, E. Ali, C.G. Ning, J. Colgan, O. Ingólfsson, D.H. Madison, M.J. Brunger, J. Chem. Phys. 145 (2016), 164306.
- [23] E. Wang, X. Ren, M. Gong, E. Ali, Z. Wang, C. Ma, D. Madison, X. Chen, A. Dorn, Phys. Rev. A 102 (2020), 062813.
- [24] J.D. Builth-Williams, S.M. Bellm, D.B. Jones, H. Chaluvadi, D.H. Madison, C. G. Ning, B. Lohmann, M.J. Brunger, J. Chem. Phys. 136 (2012), 024304.
- [25] E. Ali, H.S. Chakraborty, D.H. Madison, J. Chem. Phys. 150 (2012), 024303.
- [26] P. Palihawadana, J.P. Sullivan, S.J. Buckman, M.J. Brunger, J. Chem. Phys. 137 (2012), 204307.
- [27] Z. Mašín, J.D. Gorfinkiel, J. Chem. Phys. 135 (2011), 144308.
- [28] C. Winstead, V. Mckoy, Phys. Rev. A 76 (2007), 012712.
- [29] A.G. Sanz, M.C. Fuss, F. Blanco, J.D. Gorfinkiel, D. Almeida, F.F. da Silva, P. Limão-Vieira, M.J. Brunger, G. García, J. Chem. Phys. 139 (2013), 184310.
- [30] Z. Mašín, J.D. Gorfinkiel, J. Chem. Phys. 137 (2012), 204312.
- [31] G.M. Moreira, M.H.F. Bettega, J. Phys. Chem. A 123 (2019) 9132.
- [32] I.C. Walker, M.H. Palmer, Chem. Phys. 153 (1991) 169.
- [33] M.N. Pisanias, L.G. Christophorou, J.G. Carter, D.L. McCorkle, J. Chem. Phys. 58 (1973) 2110.
- [34] M. Nooijen, Spectrochim. Acta A 55 (1999) 539.
- [35] C. Fridh, L. Åsbrink, B.Ö. Jonsson, E. Lindholm, Int. J. Mass Spectrometry Ion Phys. 8 (1972) 101.
- [36] L. Åsbrink, E. Lindholm, O. Edqvist, Chem. Phys. Lett. 5 (1970) 609.
- [37] M. Oku, Y. Hou, X. Xing, B. Reed, H. Xu, C. Chang, C.-Y. Ng, K. Nishizawa, K. Ohshimo, T. Suzuki, J. Phys. Chem. A 112 (2008) 2293.
- [38] D.M.P. Holland, A.W. Potts, L. Karlsson, M. Stener, P. Decleva, Chem. Phys. 390 (2011) 25.
- [39] T. Suzuki, Faraday Discuss. 228 (2021) 11.
- [40] S.J. Cavanagh, B. Lohmann, J. Phys. B: At. Mol. Opt. Phys. 32 (1999) L261.
- [41] M.J. Brunger, W. Adcock, J. Chem. Soc. Perk. Trans. 2 (2002) (2002) 1.
- [42] J. Gao, J.L. Peacher, D.H. Madison, J. Chem. Phys. 123 (2005), 204302.
- [43] D.H. Madison, O. Al-Hagan, J. Atomic, Mol. Optical Phys. 2010 (2010), 367180.
  [44] F. Ali, K. Nivon, A. Murray, C. Ning, J. Colgan, D. Madison, Phys. Rev. A 92 (2015)
- [44] E. Ali, K. Nixon, A. Murray, C. Ning, J. Colgan, D. Madison, Phys. Rev. A 92 (2015), 042711.
- [45] M. J. Frisch, G. W. Trucks, H. B. Schlegel, G. E. Scuseria, M. A. Robb, J. R. Cheeseman, G. Scalmani, V. Barone, B. Mennucci, G. A. Petersson, H. Nakatsuji, M. Caricato, X. Li, H. P. Hratchian, A. F. Izmaylov, J. Bloino, G. Zheng, J. L. Sonnenberg, M. Hada, M. Ehara, K. Toyota, R. Fukuda, J. Hasegawa, M. Ishida, T. Nakajima, Y. Honda, O. Kitao, H. Nakai, T. Vreven, J. A. Montgomery, J. E. Peralta, F. Ogliaro, M. Bearpark, J. J. Heyd, E. Brothers, K. N. Kudin, V. N. Staroverov, R. Kobayashi, J. Normand, K. Raghavachari, A. Rendell, J. C. Burant, S. S. Iyengar, J. Tomasi, M. Cossi, N. Rega, J. M. Millam, M. Klene, J. E. Knox, J. B. Cross, V. Bakken, C. Adamo, J. Jaramillo, R. Gomperts, R. E. Stratmann, O. Yazyev, A. J. Austin, R. Cammi, C. Pomelli, J. W. Ochterski, R. L. Martin, K. Morokuma, V. G. Zakrzewski, G. A. Voth, P. Salvador, J. J. Dannenberg, S. Dapprich, A. D. Daniels,

- Ö. Farkas, J. B. Foresman, J. V. Ortiz, J. Cioslowski and D. J. Fox, Gaussian 09, Revision B.01, Gaussian Inc., Wallington CT, USA (2010).

  [46] J.P.D. Cook, C.E. Brion, Chem. Phys. 69 (1982) 339.

  [47] J.V. Ortiz, V.G. Zakrzewski, J. Chem. Phys. 105 (1996) 2762.

  [48] S. Xu, X. Ma, S. Yan, P. Zhang, J. Chem. Phys. 136 (2012), 237101.

- [49] D.B. Jones, J.D. Builth-Williams, S.M. Bellm, L. Chiari, H. Chaluvadi, D. H. Madison, C.G. Ning, B. Lohmann, O. Ingolfsson, M.J. Brunger, Chem. Phys. Lett. 572 (2013) 32.
- [50] G.B. da Silva, R.F.C. Neves, L. Chiari, D.B. Jones, E. Ali, D.H. Madison, C.G. Ning, K.L. Nixon, M.C.A. Lopes, M.J. Brunger, J. Chem. Phys. 141 (2014), 124307.